[10]Cheng, S.C. and Vachon, P.I., "A Technique for Predicting the Thermal Conductivity of Suspension, Emulsions, and Porous Materials," *International Journal of Heat and Mass Transfer*, Vol. 13, March 1970, pp. 537-546.

Criteria for the Evaluation of Laser Solar Energy Converter Systems

W.L. Harries*
Old Dominion University, Norfolk, Virginia

I. Introduction

ONE concept for collecting solar energy is to use large solar collectors on orbiting space stations, which then transmit the energy as laser beams. Direct conversion by solar pumped gas lasers has already been considered and the power conversion efficiency disscussed.[1-3] However, a figure of merit, of more importance for space missions, is the output power per unit weight ratio.

An idealized energy conversion system is shown in Fig. 1. The solar radiance is collected in a parabolic reflector and, for a required output power, its area is determined by the laser efficiency. The power not converted into the laser beam must be dissipated by a heat radiator emitting by Stefan's Law which, as the converter efficiency is usually low, will contribute the major part of the total weight of the system.

The overall efficiency of the laser can be decomposed into the product of several efficiencies, which affect the collector and radiator in different ways. The efficiencies are described in Sec. II and the energy flow is discussed in Sec. III. The dependencies of weight on area are then assumed, which determine the weight for a given output power. Some comparisons will be shown of different laser systems.

II. Efficiency of Solar Pumped Lasers

The overall efficiency of solar pumped lasers can be subdivided into the product of four efficiencies.[1] First, it aborption occurs over a bandwidth λ_1 to λ_2, the fraction of the solar spectrum used, or "solar utilization efficiency," is η_S,

$$\eta_S = \int_{\lambda_1}^{\lambda_2} \Phi(\lambda)\mathrm{d}\lambda \Big/ \int_0^{\infty} \Phi(\lambda)\mathrm{d}\lambda$$

where $\Phi(\lambda)$ is the solar radiance in photons per square meter between λ and $\lambda + \mathrm{d}\lambda$.

The absorption efficiency η_A is that fraction of photons within the absorption bandwidth absorbed by the gas: $\eta_A = 1 - \exp(-\sigma_a(N)\mathrm{d})$, where σ_a is the absorption cross section, (N) the density of absorbers, and d the thickness of gas.

Of the photons absorbed, only a fraction, η_K, end up producing a lasing transition. The kinetic efficiency η_K is determined by the detailed kinetics of the laser and, for example, it takes accounts of losses in the upper laser level due to quenching, etc.[2,3] Finally, the quantum efficiency η_Q is the ratio of the energy of the emitted photon to the average energy of the absorbed photons.

The device efficiency would then be $\eta_D = \eta_A\eta_K\eta_Q$, and the overall solar efficiency $\eta = \eta_S\eta_A\eta_K\eta_Q$, which is usually an order of magnitude less than η_D.

Received Nov. 20, 1984; Technical Note received April 22, 1985.

*Professor, Department of Physics.

III. Energy Flow in Solar Pumped Lasers

The energy flow for the idealized model in Fig. 1 is shown in Fig. 2. The solar power falling on the collector of area A_c is P_i. The mirror of reflectivity r concentrates the flux, and a fraction rP_i reaches the first transparent wall containing the lasing medium. However, a fraction $(1-r)P_i$ has been absorbed by the mirror and has to be radiated. The first container wall is assumed to have a transmittance τ_1, so the power arriving at the lasing medium is $\tau_1 rP_i$, and the power absorbed by the wall is $(1-\tau_1)rP_1$, which also has to be radiated.

The power arriving at the laser medium is distributed in wavelength over the solar spectrum; only a fraction, η_S, can be utilized, and of that only η_A is absorbed. The power absorbed P_A is $\eta_S\eta_A\tau_1 rP_i$ and the output power P_O is $\eta_K\eta_Q P_A$, while the part lost due to the lasing process, $(1-\eta_K\eta_Q)P_A$, has to be radiated. The power not absorbed by the lasing medium is $(1-\eta_S\eta_A)\tau_1 rP_i$ and reaches the second wall of transmittance τ_2. Then $\tau_2(1-\eta_S\eta_A)\tau_1 rP_i$ is transmitted through it, but an amount $(1-\tau_2)(1-\eta_S\eta_A)\tau_1 rP_i$ absorbed in the wall has to be radiated.

The total power that has to be radiated is P_r

$$P_r = P_i\{(1-r) + r(1-\tau_1) + r\tau_1\eta_S\eta_A(1-\eta_K\eta_Q) + r\tau_1(1-\eta_S\eta_A)(1-\tau_2)\} \quad (1)$$

As the output power P_O and input power P_i are related by $P_O = r\tau_1\eta P_i$, the relation between the radiated and output power is

$$P_r = KP_O/\eta \quad (2)$$

where

$$K = (1/r\tau_1)[(1-r) + r(1-\tau_1) + r\tau_1\eta_S\eta_A(1-\eta_K\eta_Q) + r\tau_1(1-\tau_2)(1-\eta_S\eta_A)] \quad (3)$$

IV. Output Power to Weight Ratio

The solar irradiance I_0 is 1.4 KWm^{-2}, and if the output power is $P_O(kW)$, then the area of the collector $A_c(m^2)$ *is*

$$A_c = P_O/(I_0\eta r\tau_1) \quad (4)$$

The radiator emits by Stefan's Law and its area is

$$A_r = P_r/\sigma\epsilon T^4 \quad (5)$$

where σ is Stefan's constant, ϵ the emissivity, and T, the temperature of the emitting surface. It is assumed that efficient conduction by heat pipes causes T to approach the work-

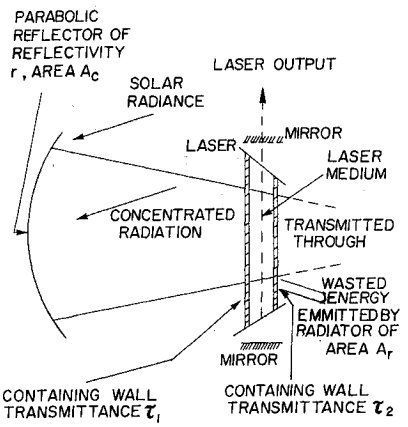

Fig. 1 Idealized arrangement for a solar pumped laser.

Table 1 Comparison of various lasing materials in solar pumped lasers

Material	η_S	η_A	η_K	η_Q	η	T,K	P_O/W $\beta/\alpha=1$	P_O/W $\beta/\alpha=10$
IBr	0.12	1	0.57	0.18	1.2×10^{-2}	423	1.2×10^{-2}	4.4×10^{-3}
C_3F_7I	10^{-2}	1	1	0.22	2.2×10^{-2}	873	2.69×10^{-3}	2.48×10^{-3}

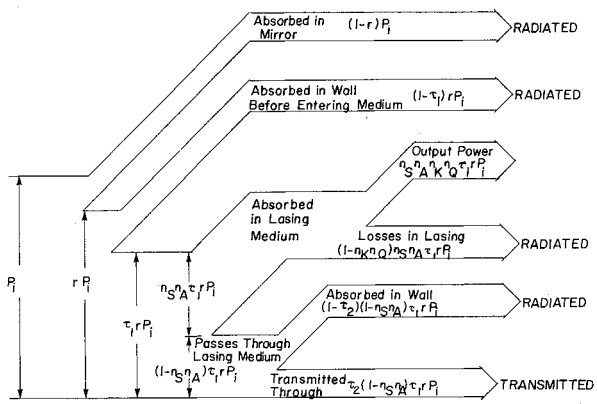

Fig. 2 Energy flow chart for a solar pumped laser.

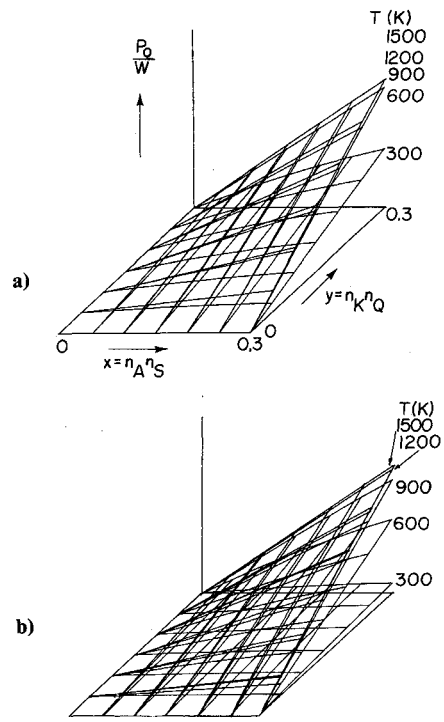

Fig. 3 Plot of P_O/W on an x,y plane for different temperatures showing effect of varying β/α. Both x and y are dimensionless, while α and β are in units of kg/m^{-2}. Values assumed are $r=0.98$, $\tau_1=\tau_2=0.9$. a) $\beta/\alpha=1$; b) $\beta/\alpha=10$, an extreme case.

ing temperature of the laser and that A_r is just sufficient to radiate the power required.

Assumptions must now be made about the dependence of the weights of the collector W_c and radiator W_r on their respective areas A_c and A_r; here, both are assumed proportional to their areas, $W_c=\alpha A_c$, $W_r=\beta A_r$, where α and β (Kgm^{-2}) are constants of proportionality. (The latter assumption may only be approximate as, for example, heat pipes may be needed to conduct to the radiator.)

The total weight W of the laser, collector, and radiator is $W=W_r+W_c+W_L$, where W_L is the weight of the laser. It is not unreasonable to assume $W_L \ll W_c$, W_r and, if so, the output power to weight ration P_O/W is

$$P_O/W=\eta/[(\alpha/1.4r\tau_1)+(\beta K/\sigma\epsilon T^4)]; \quad W_L \ll W \qquad (6)$$

Assuming that α and β, which are determined by structure design, are constants for all lasers, then Eq. (6) enables a comparison to be made for different lasing materials, provided the various efficiencies at the working temperatures are known. For fixed α, we may also make comparisons in terms of β/α. The dependence on the efficiencies is $P_O/W=f(x,y)$, where $x=\eta_S\eta_A$ and $y=\eta_K\eta_Q$. A plot of P_O/W on an xy plane is shown in Fig. 3, for $r=0.98$, $\tau_1=\tau_2=0.9$. (The value 0.9 is achievable if the walls are either KCs or CsI.[4]) The values of β/α are taken as 1 and 10, the latter being an extreme case for illustrative purposes. The range of x and y is only 0-0.3, corresponding to actual efficiencies in practice; $\epsilon=0.9$, and $300\leq T\leq 1500$ K.

For both cases P_O/W is either constant or increases monotonically with both x and y. The effect of β/α is large at low temperatures, (comparing Fig. 3a and 3b) and here $P_O/W\tilde{\propto}1/\beta$. At high temperatures, the T^4 dependence quickly makes the area required for the radiator small, and P_O/W is independent of both T and β/α, provided T is high.

A comparison of IBr and C_3F_7I lasers is shown in Table 1. It is assumed that the gas pressure and depth are sufficiently high, $\eta_A=1$. The kinetic efficiency of C_3F_7I is assumed as 1. The value of P_O/W, is calculated from Eq. (6), assuming $r=0.98$, $\tau_1=\tau_2=0.9$, $\alpha=1$. The temperatures are approximate working temperatures. Table 1 shows that the IBr laser has a power/weight ratio several times higher than the C_3F_7I laser for $\beta/\alpha=1$ and 10.

V. Conclusion

Assuming that a laser solar energy converter has a radiation collector and heat emitter whose weights are proportional to their areas, and that the weight of the laser is negligible in comparison, the output power per unit weight can be expressed in terms of the efficiencies and working temperatures of the system. This ratio seems to be several times higher for an IBr than a C_3F_7I laser because η_S is greater for the former, although the working temperature is lower. However, future converters should operate both at high efficiencies and at high temperatures.

Acknowledgments

The work was supported by Grant NSG-1568 from NASA Langley Research Center, Hampton, Virginia. The author acknowledges many useful discussions with Dr. J.H. Lee of NASA Langley, who first pointed out the significance of the power-to-weight ratio.

References

[1]Harries, W.L. and Wilson, J.W., "Solar-Pumped Electronic-to-Vibrational Energy Transfer Lasers," *Space Solar Power Review*, Vol. 2, April 1981, p. 367.

[2]Harries, W.L. and Meador, W.E., "Kinetic Modeling of an IBr Solar Pumped Laser," *Space Solar Power Review*, Vol. 4, No. 3, Sept. 1983, p. 189.

[3]Lee, J.H. and Weaver, W.R., "A Solar Simulator-Pumped Atomic Iodine Laser," *Applied Physics Letter*, Vol. 39, July 1981, p. 137.

[4]Taussing, R., Bruzzone, C., Nelson, L., Quimby, D., and Christiansen, W., *Proceedings, of the AIAA Terrestrial Energy Systems Conference,* Orlando, FL, June 4-6, 1979, pp. 1-17.

Vortex Shedding Studies in a Simulated Coaxial Dump Combustor

R. S. Brown,* R. Dunlap,† S. W. Young,‡ and R. C. Waugh§
United Technologies, San Jose, California

PERIODIC shedding of vortices produce in highly sheared flows has been recognized as a source of substantial acoustic energy for many years. Flandro and Jacobs[1] were the first to suggest that this source of energy could be a significant contributor to acoustic instabilities in some solid propellant rocket motors. Subsequently, experimental studies by Brown et al.[2] demonstrated that vortex shedding from restrictors in large, segmented, solid propellant rocket motors couples with the chamber acoustics to generate substantial acoustic pressures. The maximum acoustic energies were produced when the shedding frequency matched one of the acoustic resonances of the combustor. Additional studies[3-5] demonstrated that the location of the restrictors on the acoustic mode is also important; in particular, that the maximum acoustic pressures are generated when the restrictors are located near a velocity antinode.

In addition to a segmented solid propellant rocket motor, highly sheared flow separations can be generated in a wide variety of rocket motor and ramjet engine designs. One such geometry is the sudden flow-area expansion found at the dump plane of coaxial-inlet ramjet engines and at the grain transition in boost/sustain-type tactical solid propellant rocket motors. Thus, it is conceivable that periodic vortex shedding could be a significant source of acoustic energy in these types of combustors as well.

To examine this possibility, in 1981, a test program was initiated using the cold-flow apparatus shown schematically in Fig. 1. This apparatus simulates the grain transition in a boost-sustain-type solid propellant rocket. In addition, it roughly approximates the inlet dump region of a coaxial-inlet solid-fuel ramjet engine. Approximately 33% of the nitrogen entered through a choked 5-cm-diam inlet, while the remaining flow entered laterally through a 10-cm-diam porous bronze tube downstream of the dump plane. The lateral flow was choked by a concentric flow-distribution tube upstream of the porous bronze tube; the same method was used in the segmented motor studies.[2] A Kistler pressure transducer was mounted just upstream of the choked exhaust nozzle and a single-element hot-wire anemometer was mounted through the dump plane to measure the mean and oscillatory flows in the recirculation zone. All tests were conducted at 275 kPa (40 psia) at the entrance plane to the exhaust nozzle.

Received Feb. 10, 1985; revision received May 29, 1985.

*Senior Staff Scientist, Chemical Systems Division. Associate Fellow AIAA.
†Senior Staff Scientist, Chemical Systems Division. Member AIAA.
‡Research Engineer, Chemical Systems Division.
§Senior Research Engineer, Chemical Systems Division.

The first tests were conducted to determine if significant acoustic pressures could be generated in this type of geometry. The Mach number at the nozzle entrance (and, hence, the vortex-shedding frequency) was varied from 0.06 to 0.25 by changing the diameter of the exhaust nozzle. Figure 2 shows the rms acoustic pressure at the exhaust nozzle as a function of Mach number. The significant increase in acoustic pressure for $0.14 < M < 0.15$ was accompanied by clearly audible tones from the exhaust. These tones were not observed at the other Mach numbers.

Figure 3 shows the corresponding mean and oscillatory Mach numbers in the recirculation zone. Both recirculation Mach numbers maximize at the chamber Mach numbers where the acoustic pressures are also a maximum. The peak in mean speed is surprising at first; however, it is consistent with the intrusion of the edge of the vortex into the recirculation zone. Thus, these results indicate that periodic shedding of a vortex structure is responsible for the flow oscillations and acoustic pressures.

Figure 4 shows the frequency spectra of the acoustic pressure for three nozzle entrance Mach numbers; two of which produced significant oscillatory levels, as shown in Figs. 2 and 3, and one which produced the low background level. Comparing Fig. 4 with Figs. 2 and 3 shows that the increased rms levels are characterized by a single dominant fre-

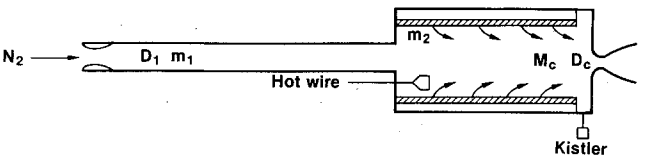

Fig. 1 Experimental apparatus.

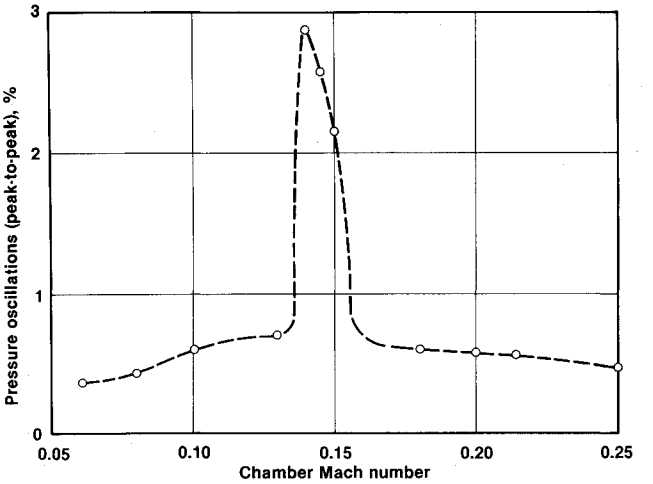

Fig. 2 Acoustic pressure levels.

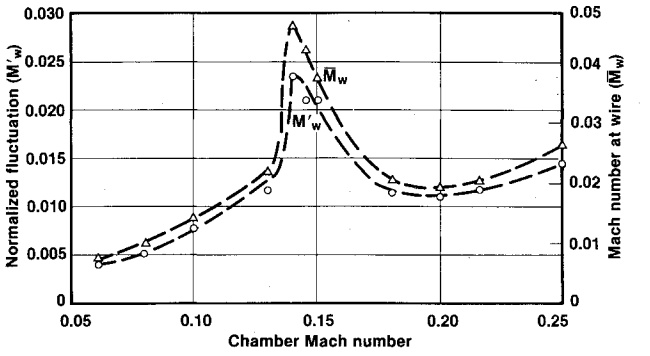

Fig. 3 Recirculation flow Mach numbers.